Hindawi
Shock and Vibration
Volume 2022, Article ID 3269604, 19 pages
https://doi.org/10.1155/2022/3269604

Research Article

Investigation of the Aerodynamic Characteristics of Platoon Vehicles Based on Ahmed Body

Jianbin Luo,[1,2] **Ke Mi**,[1,2] **Dongli Tan**,[2] **Zhiqing Zhang**,[1,2] **Mingsen Li**,[1,2] **Jun Qing**,[1,2] **and Huiqiong Huang**[1]

[1]*School of Mechanical and Automotive Engineering, Guangxi University of Science and Technology, Liuzhou 545006, China*
[2]*Institute of the New Energy and Energy-saving & Emission-reduction, Guangxi University of Science and Technology, Liuzhou 545006, China*

Correspondence should be addressed to Huiqiong Huang; huiqiongh@gxust.edu.cn

Received 27 October 2021; Revised 4 April 2022; Accepted 15 April 2022; Published 1 June 2022

Academic Editor: Zengshun Chen

In this paper, the aerodynamic characteristics of two vehicles and three vehicles in the platoon under different vehicle spacings have been explored in detail. Firstly, the realizable k-ε model was used to verify the numerical method based on a single 35° Ahmed body. Then, the aerodynamic characteristics such as drag characteristics, surface pressure, wake structure, and turbulent kinetic energy distribution were analyzed for the platoon of two and three 35° Ahmed bodies. Although the RANS (Reynolds-averaged Navier–Stokes) model had got good results for simulating a single 35° Ahmed body, when simulating two 35° Ahmed bodies in the platoon, it was found that there is still a big error compared with the experimental data. In the three 35° Ahmed body, the drag coefficient of the leading body is almost unchanged compared with that of the leading body in the two-vehicle platoon, while the drag coefficients of the middle body and the trailing body are both reduced compared with those of the single body. For $x/L = 0.25$, the middle body is about 56% of the single-body value, and the trailing car is about 88% of the single-body value. It can be seen that the drag reduction effect of three 35° Ahmed bodies is larger than that of two 35° Ahmed bodies. It is shown that the aerodynamic characteristics are very sensitive to the selected platoon vehicle model. Because model with different geometric shapes will produce different wake structures, different aerodynamic phenomena will occur when they are arranged in the platoon.

1. Introduction

At present, people have realized that global warming will bring serious environmental damage, and governments and relevant institutions all over the world have formulated strict laws and regulations to control this damage [1]. However, for the automobile industry, there are still great challenges, and the environmental pollution caused by automobile exhaust is still very serious. Therefore, the research on exhaust emission treatment is becoming more and more important [2]. With the development of economy, energy saving and emission of motor vehicles have become issues of concern to everyone [3]. Some people can better control pollutant emissions by evaluating the emission characteristics of nitrogen oxides from different aspects [4–9]. In addition, automobile aerodynamics also plays a very important role in improving fuel economy and controlling emissions. It uses aerodynamic characteristics to optimize the shape of a single vehicle, thereby reducing vehicle drag and achieving the goal of saving fuel consumption and reducing exhaust emissions. However, the research on the aerodynamics of multiple vehicles traveling close to each other is becoming more and more popular, because the aerodynamic characteristics between vehicles at a close distance not only improve the transportation rate, but also save fuel consumption and reduce exhaust emissions under the advantage of reduced drag. This type of arrangement is generally called platooning. "Platoon" is the term used by the Federal Highway Administration (FHWA) Intelligent Vehicle Highway System (IVHS) project. In this project, a group of 10–20 vehicles traveled longitudinally at a small distance at a speed of 65–70 miles per hour, which may not only greatly improve the traffic capacity of expressways, but also reduce fuel costs and exhaust emissions [10]. Therefore,

this will also be an important part of the development of intelligent transportation systems in the future. At present, the research of reducing the average drag by one car following another car does not only appear in automobiles. For example, in cycling [11], birds flying [12], and motor racing [13], it is to reduce drag or energy consumption by means of platooning.

When vehicles are traveling in a row for a short distance, the leading vehicle is equivalent to a shield, blocking the impact of the airflow for the following vehicles, and then the drag coefficient of the following vehicle will be greatly reduced. In order to improve the rapid growth of traffic congestion, air pollution, and energy consumption in California, the Partners for Advanced Transit and Highways (PATH) proposed and studied an automated highway system (AHS) [14]. In this system, the highway capacity can be achieved by increasing the number of vehicles in the platoon (from 2 to 6), and then these vehicles travel at the same speed with a smaller distance [15]. Michael Zabat et al. [10] used a 1/8 scale model of a standard American minivan to conduct a wind tunnel test to study the effect of vehicle spacing on the drag of each vehicle in 2, 3, and 4 vehicles in the platoon. For distances less than one vehicle length, the drag coefficients of all vehicles in the platoon were reduced, although the reduction of internal vehicles was even greater. When the distance was half the length of the vehicle, the average drag coefficient of the four vehicles in the platoon was reduced to 0.62 times that of the nonplatoon traveling. Then, people conducted real-vehicle experiments on the trucks or trucks in the platoon [16–19]. The research results all showed that it could indeed bring about the effect of saving fuel consumption when traveling at close distances. Of course, there are also numerical simulations [20, 21] and wind tunnel experimental studies [22, 23] using truck or truck models. Prasad Vegendla et al. [24] used the truck model through numerical simulation to not only study the aerodynamic characteristics caused by the longitudinal spacing, but also study the situation under the lateral spacing. However, the main concern under lateral spacing was the safety and handling stability of running vehicles. Paolo Schito et al. [25] studied the influence of the shape of the vehicles in the platoon and the relative distance between the vehicles. The results showed that the drag of vehicles with an estate back such as station wagons and sport utility vehicles was reduced by more than 50% when traveling in a platoon. While a fastback vehicle like a sedan had better aerodynamic performance than other vehicles when traveling alone, the advantage of drag reduction when traveling in a platoon is not as good as that of the estate back vehicles. When a truck was traveling in a platoon with other vehicles, the drag reduction trend of the truck was almost small, while the drag reduction of the vehicles behind the truck was very high. However, David Uystepruyst et al. [26] studied the large eddy simulation of the flow around a four-car platoon when a member of the vehicle platoon was forced to oscillate in a straight line. Based on steady-state research, the aerodynamic characteristics changes of the third model of the four cuboid models at different spacings before and after are analyzed. Kim et al. [27] used the SolidWorks Flow Simulation tool to study the variation and causes of drag coefficients caused by four different vehicle models traveling in a platoon with different intervehicle distances. Bounds et al. [28] studied an extension of the method for numerical simulation of vehicle platooning. First, the ability of the turbulence model in the CFD simulation of vehicle platooning to predict aerodynamics is explored, and then the method of vehicle platooning simulation is developed by using cube model, which finally extends to the aerodynamic characteristics produced in the platoon by the realistic vehicle model DrivAer. Jaffer et al. [29] used a machine learning algorithm to predict drag coefficients on vehicle platoon. The drag coefficients for each vehicle in a two-, three-, and four-vehicle platoon were predicted from experimental study data provided at different inter-vehicle distances in a platoon, and the predicted values were compared with numerical simulation results. Finally, it is concluded that the polynomial regression model in mechanical learning algorithm is the most consistent with the aerodynamic prediction. From the research introduction of the above report, it can be found that the research on the shape of the vehicle in the platoon traveling is very important, whether in the case of the same shape of vehicles or the combination of different shapes of vehicles. Because different vehicle shapes will produce different flow structures, they will also have different effects when traveling in a platoon. At present, most of the research is to use simplified vehicle models [30–33], and only a few authors have studied representative passenger car models [34].

However, it has been reported that there are some differences in drag coefficient changes when following a car at close distances under certain conditions. At $x/L < 0.35$ (where x and L appearing here and below are the inter-vehicle distance and vehicle length, respectively), Michael Zabat et al. [35] found that the drag coefficient of the trailing vehicle was higher than that of the leading one. For the Ahmed model, the above situation is more intense. In the range of $x/L = 0$–1, the drag of the following vehicle is always higher than that of the leading vehicle and the single one [36–39], and then some numerical simulation studies have shown the same results [40–42]. Altinisik et al. [43] used the one-fifth scale model FIAT Linea to conduct a numerical simulation study of a two-vehicle platoon. They also found that the drag coefficient of the leading vehicle increased significantly at the distance between $x/L = 0$ and 0.5, while the drag coefficient of the trailing vehicle was slightly higher than that of the single one. In the platoon vehicle study, Hesham Ebrahim et al. [34] used a quarter-scale model of the 2016 hatchback Nissan Leaf, and it was found that in the two-vehicle platoon, when the distance $x/L = 0.25$, the drag of the trailing vehicle suddenly increased and was higher than that of the single one. However, it was found that the drag of all vehicles in the three-vehicle platoon was lower than that of the single vehicle. At the same time, Browand et al. [44] used two simplified geometric shapes as truck models for experimental research. Under different geometric combinations, it was found that when the truck model with a sharp front edge was used as the leading vehicle, the drag coefficient of the trailing vehicle would be higher than that of a single truck model.

The research on automobile aerodynamics in the platoon can be roughly divided into three aspects: vehicle spacing, number of vehicles, and shape of vehicles. At present, the research of vehicle platoon is mainly affected by the lack of experimental equipment, the actual vehicle experiment will be restricted by the road, and the model experiment may be restricted by the length of the wind tunnel test section. Therefore, most of the existing experimental studies are aimed at the short distance and the small number of vehicles. In recent years, with the development of computer technology, numerical simulation methods have made great progress and become a good supplement to wind tunnel tests. Nevertheless, it is still not easy to obtain an accurate simulation of the flow field outside the ground vehicle. The flow structure of the vehicle external flow field is very complex, and the flow characteristics of airflow are irregular, so the accuracy of external flow field simulation is affected by many factors. Although the current large eddy simulation (LES) [45] and detached eddy simulation (DES) [46] have obtained good results in numerical simulation, their huge computational cost has to be considered. Therefore, Reynolds-averaged Navier–Stokes (RANS) simulation is quite popular for studying the change of average aerodynamic characteristics caused by vehicle platoon at present. This paper is mainly based on the steady-state realizable k-ε model for numerical simulation research, Ahmed body as the research model of this article. For the Ahmed body platoon, many scholars have already conducted this kind of research. However, their research contents are all carried out on two Ahmed bodies. The rounded head and slanted tail of the Ahmed body result in a different aerodynamic phenomenon in the platoon than that of the conventional vehicle model platoon. Therefore, this paper extends the platoon study of three Ahmed bodies to investigate the effect of aerodynamics when increasing the number of vehicles in the Ahmed body platoon. Then, analyze the differences in aerodynamic characteristics with the two Ahmed body platoons and the conventional vehicle model platoons with increasing number of vehicles.

2. Governing Equations

In the simulation calculation of automobile external flow field, air can be considered as an incompressible flow [47]. Because the airflow speed of 90 Km/h selected in this study is far lower than the sound speed, its Mach number (ratio of airflow speed to local sound speed) is less than 1, and the influence of temperature on the flow field is not considered. Therefore, the governing equations to be solved include continuity equation, momentum equation, turbulent kinetic energy k equation, and turbulent dissipation rate ε equation. Combined with the boundary conditions of the flow field, the unknown velocity, pressure, turbulent kinetic energy, and turbulence dissipation rate in the equations can be solved, so as to obtain the solution of the entire flow field. The specific control equation is as follows:

Mass conservation equation (continuity equation):

$$\frac{\partial u_i}{\partial x_i} = 0. \tag{1}$$

Momentum conservation equation (Reynolds-averaged Navier–Stokes equation):

$$\frac{\partial}{\partial x_j}\left(\rho\overline{u_i u_j}\right) = -\frac{\partial \overline{p}}{\partial x_i} + \frac{\partial}{\partial x_i}\left(\mu\frac{\partial u_i}{\partial x_j} - \overline{\rho u_i u_j}\right), \tag{2}$$

k equation:

$$\frac{\partial(\rho k u_i)}{\partial x_i} = \frac{\partial}{\partial x_j}\left[\left(\mu + \frac{\mu_t}{\sigma_k}\right)\frac{\partial k}{\partial x_i}\right] + G_k - \rho\varepsilon, \tag{3}$$

ε equation:

$$\frac{\partial(\rho\varepsilon u_i)}{\partial x_i} = \frac{\partial}{\partial x_j}\left[\left(\mu + \frac{\mu_t}{\sigma_\varepsilon}\right)\frac{\partial \varepsilon}{\partial x_i}\right] + \rho C_1 E\varepsilon - \rho C_2\frac{\varepsilon^2}{k + \sqrt{\nu\varepsilon}}, \tag{4}$$

where u_i and u_j are the velocity components of coordinates x, y, and z, respectively, m/s; and x_i, x_j are the coordinates x, y, and z, where i and $j = 1$, 2, and 3. ρ are the density of the fluid medium, kg/m^3; P are the pressure of the fluid medium Pa; μ is the dynamic viscosity, Pa·s; μ_t is turbulent viscosity coefficient; ν is kinematic viscosity, m^2/s; E is strain rate, s^{-1}; G_k is the generation term of turbulent kinetic energy k caused by average velocity gradient; σ_k and σ_ε are Prandtl numbers corresponding to turbulent kinetic energy k and dissipation rate ε, respectively; and C_1 and C_2 are the model coefficients.

3. Selection and Verification of Numerical Simulation Method

3.1. Simulation Model and Computational Domain. The surface modeling of the real automobile model is complicated, and the bottom structure is irregular, so it is often simplified in the numerical simulation. Ahmed model was a kind of car-like model proposed by SR Ahmed et al. [48] in 1984. Ahmed model is composed of a round front, a variable slant at the rear of the car body, and a cuboid connecting the front and rear slant. The variable slant at the rear is mainly used to study the drag coefficient and wake separation phenomenon of the car body at different slanted angles. Although the model is simple, it retains the basic characteristics of automobiles and can accurately reflect the flow field around automobiles. In the numerical simulation in this paper, the Ahmed model with a rear slanted angle of 35° is selected. The solid modeling shape is shown in Figure 1, and the main structure size is shown in Figure 2.

In the simulation calculation, the cuboid computational domain is used. The entrance distance is twice as long as the Ahmed model, the exit distance is six times as long as Ahmed model, the distance from top to bottom is six times as high as Ahmed model, the distance from left to right is seven times as wide as Ahmed model, and the ground clearance is 50 mm, as shown in Figure 3. At this time, the blocking ratio is 2%, which is less than 4% in the literature [49], so the blocking effect of the wind tunnel can be ignored. In addition, the calculation domain sizes of the front, rear, left, and right, and up and down of the car body are the same, regardless of the single-vehicle traveling condition or the platoon condition.

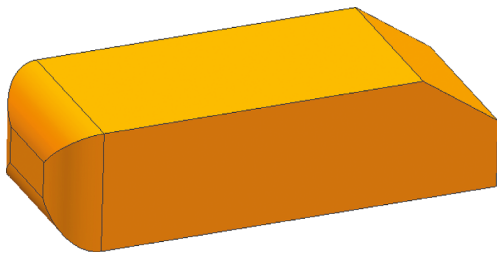

Figure 1: Ahmed body.

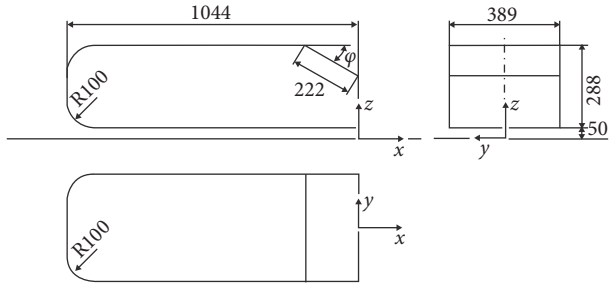

Figure 2: Geometric dimensions of the model (unit: mm).

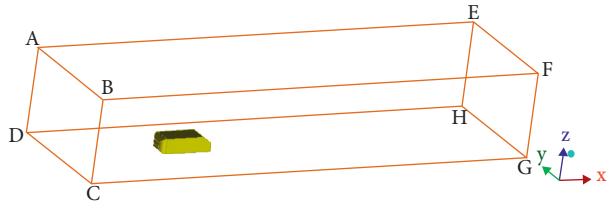

Figure 3: Computational domain and coordinate system.

3.2. Grid Division and Mesh Independence Verification. Grid division is extremely important for simulation calculation, and the type and accuracy of mesh directly affect the calculation time and accuracy. The geometric shape of Ahmed body is relatively regular and simple. Therefore, using a better quality hexahedral structured mesh, but the curvature of its body head is large and blunt, so it is difficult to capture the structure. Therefore, after creating an O-block structure around the whole body, it is necessary to create a C-block structure on its head separately, which can better capture the Ahmed body head structure. Finally, in order to better refine the mesh around the body, after the O-block structure is generated around the car body, then a layer of C-block structure is generated. Finally, the generated mesh looks at Mesh 1 in Figure 4.

Generally speaking, the more the total number of mesh cells, the higher the accuracy will be, and it is easier to capture the detailed features of the object surface. However, the more mesh number there are, the more computing time and memory are needed, and the higher the computing configuration will be, and computing time and computer hardware resources are limited. Therefore, in practical applications, it is necessary to strike a balance between calculation time and calculation accuracy. The following five sets of mesh types are used for mesh independence verification, and all five sets of meshes adopt the same topology structure, as shown in Figure 4.

Table 1 compares the drag coefficients of the five sets of grids with the results of the literature [39]. It can be seen from the table that there is a certain relationship between the simulation results and the total number of mesh cells, and there is a big difference between the calculated values of drag coefficient with less meshes and those with more meshes. The calculation results of Mesh 4 and Mesh 5 are very similar, and the error with the experimental data is the smallest. Since this study is a three-vehicle platoon, the calculation mesh number will increase with the increase of the vehicle spacing. Considering the configuration limit of this computer, Mesh 3 is adopted as the mesh scheme of this study.

3.3. Boundary Layer Analysis. Studies have shown that the flow in the boundary layer can be divided into three sublayers: viscous bottom layer, transition layer, and logarithmic law layer [50]. In order to better simulate the viscous flow in the boundary layer, the wall function method is used for approximate solution; that is, the physical quantities in the near-wall region are directly related to those in the turbulent core region by using semiempirical formula. The

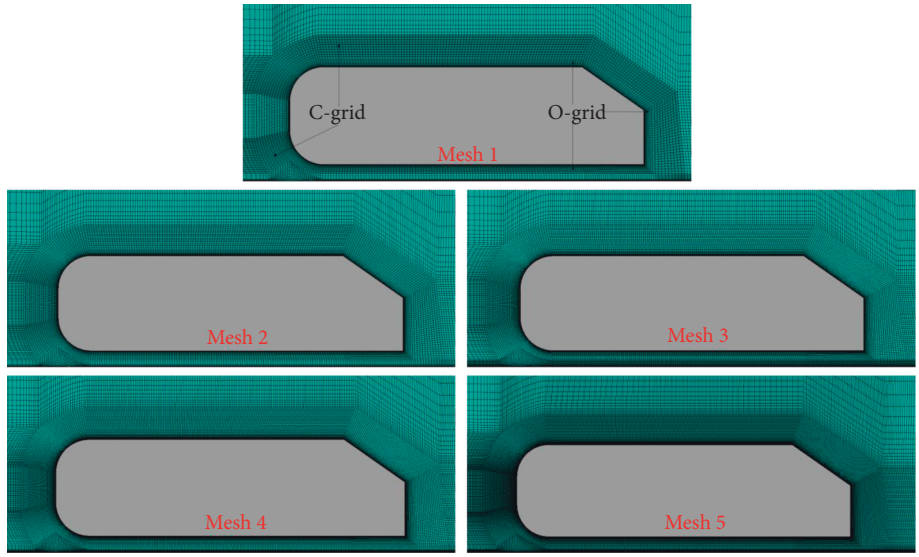

Figure 4: Schematic diagram of five sets of grids on the *xz* symmetry plane.

Table 1: Mesh independence verification.

Mesh type	Cell size of body surface (mm)	The total number of mesh cells	CFD C_D	Exp C_D
Mesh 1	8	1.65 million	0.2837	
Mesh 2	7	2.54 million	0.2789	
Mesh 3	6	3.96 million	0.2728	0.2700
Mesh 4	5	6.00 million	0.2690	
Mesh 5	4	10.11 million	0.2694	

mesh of the wall only needs to be distributed in the region where the wall function takes effect, that is, the logarithmic law layer. In the process of CFD preprocessing, people often divide the boundary layer mesh to fully analyze the viscous sublayer. At this time, the mesh of the wall only needs to be distributed in the area where the wall function takes effect, that is, the logarithmic law layer. Therefore, it is crucial to determine the thickness of the first layer mesh. In the study of Li [51] et al., it is mentioned that the height of wall-adjacent cells is determined by estimating the thickness of viscous sublayer, and the thickness of the viscous sublayer depended on the simulation of the laminar boundary layer on the flat plate. Its formula is

$$\delta_{BL,99\%} \approx 3{\cdot}5\sqrt{\frac{2\nu l_x}{U_\infty}} \approx \frac{5{\cdot}0 l_x}{\sqrt{\mathrm{Re}_{l_x}}} = 0{\cdot}00264\ D, \tag{5}$$

where l_x is the characteristic length of the boundary layer, generally taken as 0.5D, where D is taken as the model length.

There are certain standards established for common practice in the engineering field, namely, y^+, which is a dimensionless wall distance.Through the value range of y^+, it can be judged whether the thickness of the first layer mesh is arranged in the region where the wall function takes effect. Moreover, no matter the standard k-ε model, RNG k-ε model, or realizable k-ε model, they are all aimed at fully developed turbulent flow. Therefore, when using the above turbulence model, in order to arrange the first layer mesh in logarithmic law layer, it is best to require the value range of y^+ to be 30–300. Depending on the formula (5), this paper sets 7 layers of boundary layer mesh with a grading ratio of 1.01 and estimates the thickness of the first layer mesh. Then, we can check whether the y^+ distribution is within this range through the calculation results. If not, we need to readjust the grids and calculate again. Finally, the thickness of the first layer mesh selected in this paper is 0.5 mm, and the y^+ distribution is between 22 and 78, which meets the calculation requirements.

3.4. Numerical Simulation Parameter Setup. The solver is configured as pressure-based, and the calculation is performed for steady state. The Reynolds number $\mathrm{Re} = 1.8 \times 10^6$ based on the model length, and the turbulence intensity $I = 1.8\%$. It can be seen from Table 2 that the results of the RNG k-ε model and the realizable k-ε model are very close to the experimental values, and the simulation error of the realizable k-ε model is the smallest. However, the standard k-ε model assumes that the viscosity coefficient is an isotropic scalar, while turbulence is anisotropic, and the viscosity coefficient should be an anisotropic tensor, so the calculated aerodynamic drag is too large. The RNG k-ε and realizable k-ε models both consider the rotating flow and bending flow. However, the penultimate term of ε equation in realizable k-ε model does not have any singularity. Compared with RNG k-ε model, the convergence is greatly improved, and the calculation

Table 2: Comparison of drag coefficients simulated by three turbulence models with experimental values.

Turbulence model	C_D (CFD)	C_D (EXP)	Relative error (%)
Standard k-ε	0.3481		28.93
RNG k-ε	0.2663	0.27	1.37
Realizable k-ε	0.2728		1.03

results are more accurate. Therefore, this paper chooses realizable k-ε turbulence model to calculate.

The wall function uses the nonequilibrium wall function. Because the nonequilibrium wall function takes the pressure gradient into account in the calculation, it adopts the double-layer concept to calculate the turbulence kinetic energy of the near-wall element, which has high solution accuracy for the problems of the flow field involving separation, reattachment, and other average velocities and rapid changes of pressure gradient. In this simulation calculation, the model length is selected as the characteristic length of turbulence, that is, $L = 1.044$ m. Turbulence intensity I and turbulence length scale l are selected as turbulence parameters at the inlet and outlet of the computational area, namely, $I = 1.8\%$, $l = 0.07\,L = 0.07308$. The SIMPLEC pressure-velocity coupling algorithm is adopted. The pressure interpolation is second order, and the convection term and viscosity term of the governing equation adopt the second-order discrete schemes. Solution is initialized from inlet region with set initial values. When all monitoring variables (drag force, pressure) do not change with the number of iterations of the calculation, the calculation is considered to be converged and the iteration is terminated. The boundary conditions are set as shown in Table 3.

Finally, observe the streamline diagram in Figure 5 and compare it with the experimental data in [52]. It can be seen that the realizable k-ε model has obtained good results for the wake prediction of the 35° Ahmed model, and two asymmetric vortices with different sizes in the wake formed by the upper and lower shear laminar flow are consistent with the experimental results. Although the positions of the focus point 1 (F_1) and focus point 2 (F_2) in the two vortices are deviated, the accuracy and reliability of the numerical simulation can also be verified.

4. Platoon Vehicle

4.1. Two-Vehicle Platoon. The mesh generation, turbulence model, boundary conditions, and solution parameters of the two Ahmed bodies are consistent with the calculation method settings of single body. The inter-vehicle distance of the two-vehicle platoon simulation is $x/L = 0.125$–2.

Figure 6 shows the standardized drag coefficients of two bodies at different inter-vehicle distances, and some numerical results are compared with the corresponding experimental data obtained from literature [37]. Reynolds number $\mathrm{Re} = 1.85 \times 10^6$ in the experiment (based on the model length). The drag coefficients of the leading body and the trailing body are, respectively, normalized with the drag coefficients of a single body, and this can better analyze the effect of drag coefficient vehicles in the platoon. It can be seen from Figure 6 that the simulated data and the experimental data have very similar trends, but there are large differences in the drag coefficients in individual spacing, and the maximum error of 16%. The simulation results in literature [42, 53] also have the same phenomenon. Because most RANS models cannot simulate the flow separation at the rear part, or when they predict the start of separation, they fail in a large number of separated flow regions containing many coherent structures, mainly due to insufficient prediction of turbulent stress levels [54]. Although it has obtained good results for a single 35° Ahmed body simulation prediction, for the situation in the platoon, the flow interaction between the two bodies is very strong and the flow structure is more complicated under the close inter-vehicle distances. For the three-dimensionality and instability of this turbulence, the RANS model is difficult to predict, and this phenomenon was also shown in their research [55–58].

In the range of $x/L = 0.125$–2, the drag coefficient of the trailing body is higher than that of the leading body, especially in the range of $x/L = 0.125$–1; this phenomenon is more obvious. This is because the presence of the trailing body increases the base pressure of the leading body, and the pressure difference between the front and rear of the leading body becomes smaller, resulting in a smaller drag coefficient.

For the leading body, it can be seen that the simulation results are in good agreement with the experimental data. At the spacing $x/L = 0.125$, the drag coefficient decreases to about 42% of a single body value, and with the increase of the distance, the drag coefficient begins to increase. In the range of $x/L = 0.125$–2, due to the long distance, the flow interaction between the two bodies weakened, and the drag coefficient began to become stable and approached a single body value. For a trailing car, the error between the simulated value and the experimental value is slightly larger, but the trend is consistent. In the range of $x/L = 0.125$–0.75, the drag coefficient begins to increase and is higher than a single body value. When the spacing $x/L = 0.75$, the drag coefficient reaches the peak value, which increases to about 36% higher than a single body value (while the drag coefficient in the experiment reaches the peak value at $x/L = 0.5$), and then as the distance increases, the drag coefficient began to decrease and slowly approached a single body value.

In the following flow field, pressure field, and turbulent kinetic energy distribution, only six spacings $x/L = 0.25$, 0.5, 0.75, 1, 1.25, and 1.5 are analyzed. Because in this spacing range, it just covers the process that the drag coefficient starts to increase or decrease and reaches a stable level. For the analysis method of wake phenomenology, it can include a wide array of insightful techniques such as DMD [51,59,60], SPOD [61,62], and POD [63], and other technologies like Koopman-LTI [64] and resolvent analysis [65]. This paper analyzes this wake phenomenon through the visualization of raw data. The flow velocity (U) is normalized with the inlet flow velocity (U_0). The pressure distribution is expressed by the pressure coefficient C_P, and its expression is as follows:

$$C_P = \frac{P - P_0}{0{\cdot}5\rho_0 U_0^2}, \tag{6}$$

Table 3: Setup of boundary conditions.

Boundary type	Boundary name	Corresponding values
Inlet (ABCD)	Velocity inlet	25 m/s
Outlet (EFGH)	Pressure outlet	0 Pa (equivalent to atmospheric pressure)
Ground (DHGC)	Moving wall	Slip speed 25 m/s
Ahmed body surface	Nonslip wall	—
Top (AEFB) and side walls (BFGC and AEHD)	Symmetry	—

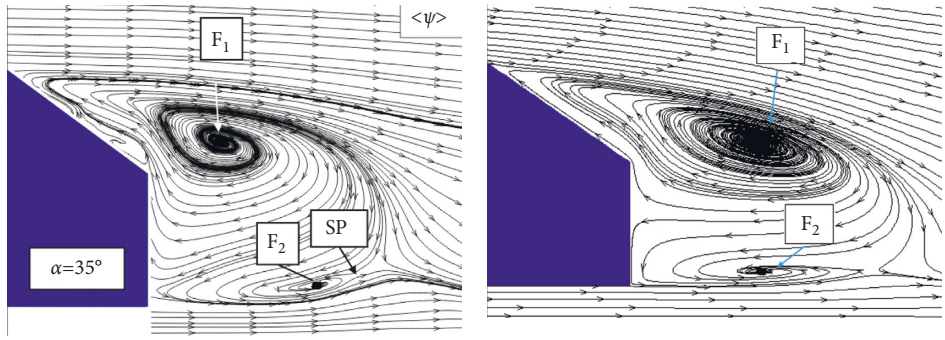

Figure 5: Comparison of tail flow field distribution on 35° Ahmed model xz symmetry plane. (a) experiment and (b) simulation.

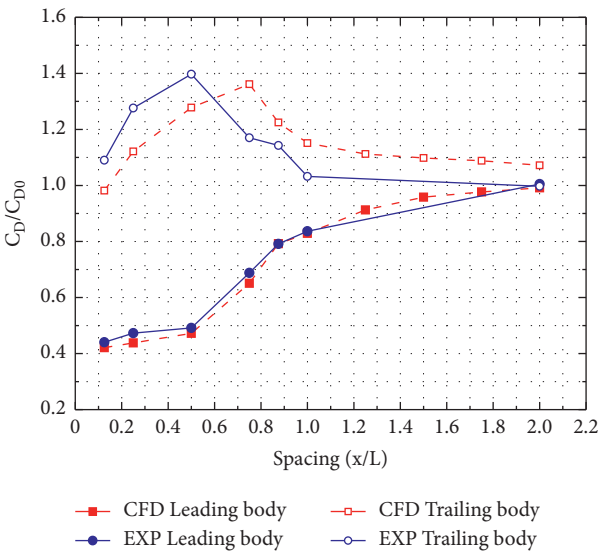

Figure 6: Normalized drag coefficient C_D/C_{D0} (C_{D0} drag value of a single body) of two Ahmed bodies under different inter-vehicle distances.

where P is pressure; P_0 is the reference pressure of free flow, which is equivalent to atmospheric pressure; ρ_0 is the density of free flow, which is equivalent to the density of air; and U_0 is the inlet free flow velocity.

Figures 7 and 8 show the x-direction velocity contour and streamline distribution between the two bodies and behind the trailing body on the xz symmetry plane. In the figures, a, b, c, d, e, and f, respectively, represent six different longitudinal vehicle spacing: (a) $x/L = 0.25$; (b) $x/L = 0.5$; (c) $x/L = 0.75$; (d) $x/L = = 1$; (e) $x/L = = 1.25$; (f) $x/L = 1.5$. The figure clearly shows the upper and lower vortices in the separated flow regions, one rotating clockwise and the other rotating counterclockwise. It can be seen from Figure 7 that for $x/L = 0.25$ and 0.5, the upper vortex between the two bodies is attached to the fore-body of the trailing body, and the impingement point of the flow is on the upper rounded edge of the trailing body's fore-body. It can also be seen that due to the close distance, the wake of the leading body has not fully developed under these two distances. Therefore, the drag coefficient of the leading body is lower than that of a single body, while the trailing body is in the wake region of the leading body, resulting in an increase in the drag coefficient of the trailing body compared with that of a single body. At x/L= 0.75, the vortex between the two bodies is not attached to the trailing body's fore-body, and the flow impingement point begins to move to the center of the trailing body's fore-body. The trailing body is still in the wake region of the leading body, but this region becomes extremely small, which leads to the peak of the drag coefficient of the trailing body. In the research of Azim and Gawad [66], it was shown that this spacing region may be related to a flow pattern called "vortex (or wake) impingement." That is, the high-energy vortex from the leading body impinges on the fore-body of the trailing body, resulting in an increase in local dynamic pressure at the fore-body of the trailing body. For $x/L = 1$, 1.25, and 1.5, due to the increase of spacing, the trailing body is completely outside the wake region of the leading body, the flow impingement point is moved to the center of the trailing body's fore-body, and there is almost no flow interaction between the two bodies. Therefore, the drag coefficient becomes stable and closer to a single body value. As for the wake region of the trailing body (Figure 8), it can be observed that the vortex region becomes smaller and smaller with the increase of inter-vehicle distances. When the spacing increases to $x/L = 1.25$ and 1.5, because the flow interaction becomes weak, the size of the vortex region no longer changes.

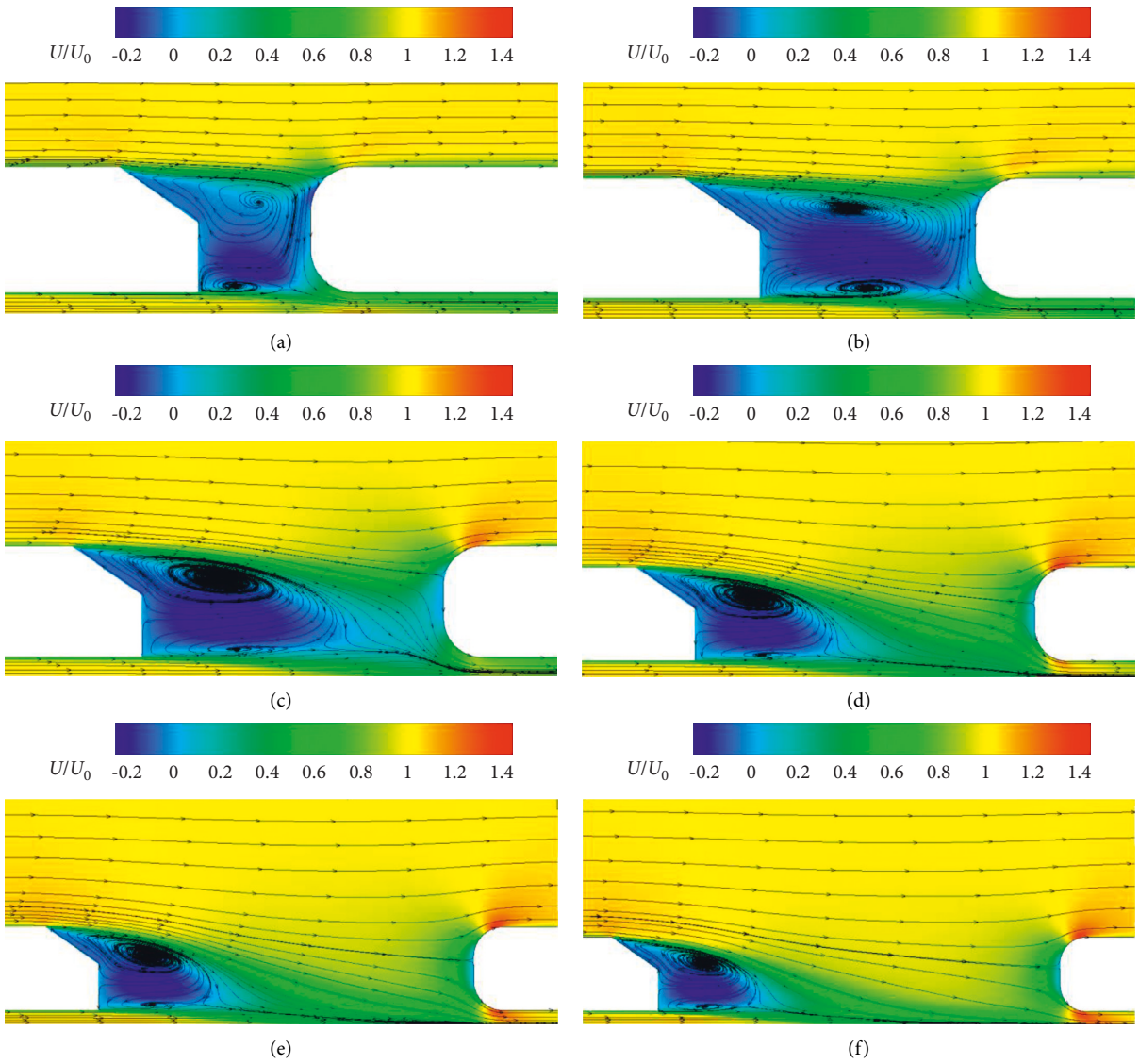

Figure 7: The x-direction velocity contour and streamline distribution between two bodies on the xz symmetry plane. (a) $x/L = 0.25$ (b) $x/L = 0.5$. (c) $x/L = 0.75$. (d) $x/L = 1$. (e) $x/L = 1.25$. (f) $x/L = 1.5$.

Figure 9 shows the pressure contour and streamline distribution of a single body and two bodies in the platoon at different inter-vehicle distances on the $z/L = 0.08$ plane. When a single body runs alone, a large positive pressure area appears at the head of the body, and a large negative pressure area appears at the rear; therefore, the body is subject to greater aerodynamic drag. At $x/L = 0.25$ and 0.5, due to the close spacing, it can be seen from the flow trajectory of the airflow that the two bodies seem to form a whole. As the spacing increases, the flow gradually penetrates into the gap between the bodies, and there is a clear streamline passing between the gaps. According to the pressure contour, as the spacing increases, the pressure distribution at the head and tail of the two bodies becomes more like that of a single body.

The change of wake structure will inevitably lead to the change of pressure. Figure 10 shows the static pressure and three-dimensional streamlines on the surfaces of two bodies at six different inter-vehicle distances, while the streamlines are colored by the x-direction velocity. Different streamline colors indicate different speeds. It clearly shows how the increase of inter-vehicle distances extends beyond the vortex region behind the leading body, and the flow impingement on the front surface of the trailing body can also be clearly seen from this figure. For $x/L = 0.25$ and 0.5, the spacing is relatively close, and then the wake of the leading body cannot fully develop. Because the upper vortex in the wake region is relatively large, most of the flow impinges the upper rounded edge of the fore-body of the trailing body (see Figures 7 and 8). This increases the base pressure of the leading body and, on the other hand, reduces the pressure in front of the trailing body. With the increase of inter-vehicle distances, the pressure in front of the trailing body will eventually increase, and the flow impingement extending from the wake of the leading body will move more and more to the center of the front surface of the trailing body. Until $x/L = 1$–1.5, the wake of the leading body can be fully

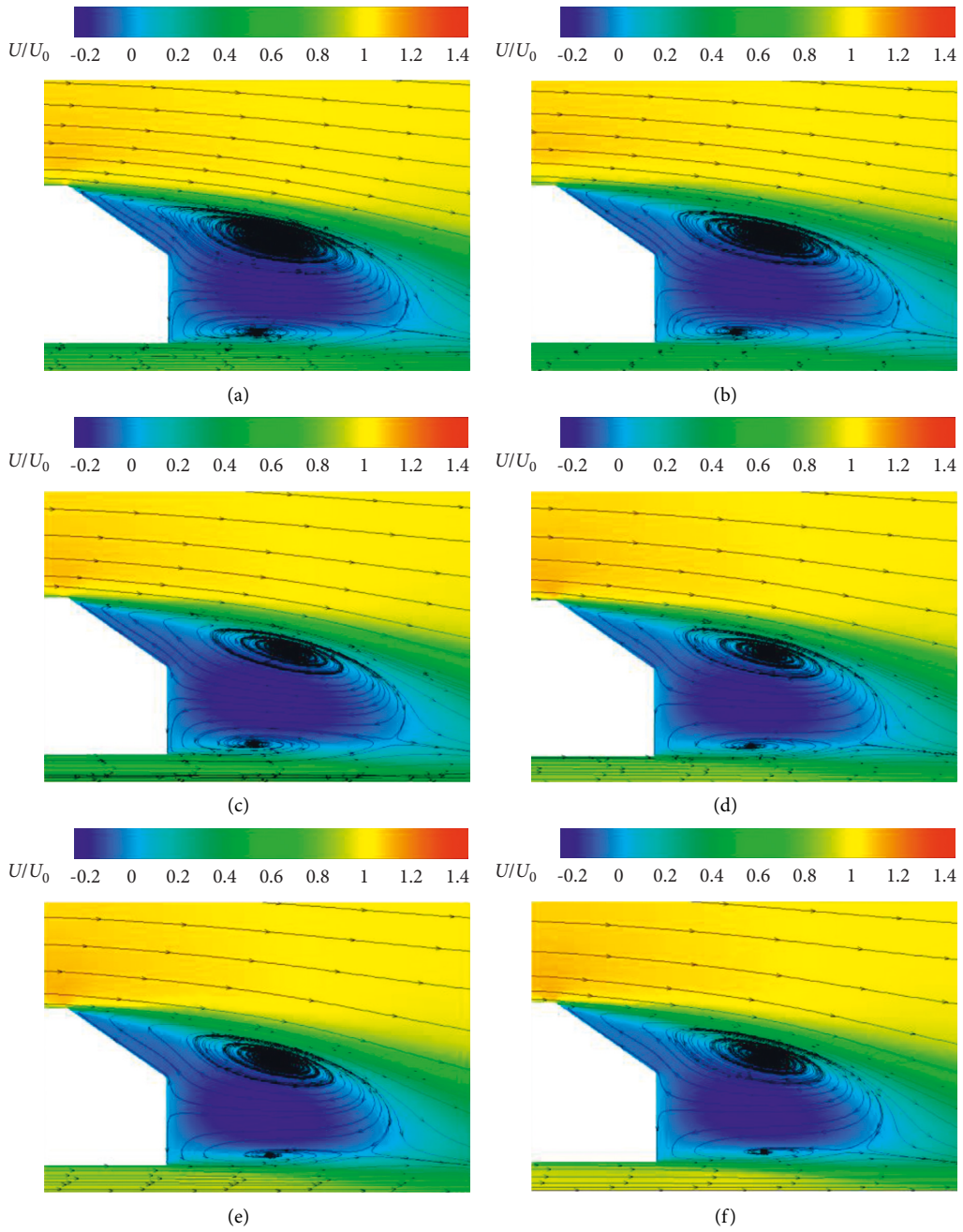

FIGURE 8: X-direction velocity contour and streamline distribution behind trailing body in two bodies on xz symmetry plane. (a) $x/L = 0.25$ (b) $x/L = 0.5$. (c) $x/L = 0.75$. (d) $x/L = 1$. (e) $x/L = 1.25$. (f) $x/L = 1.5$.

developed, the trailing body is completely outside the wake region of the leading body, and the two bodies become more independent and do not interfere with each other, so their drag coefficients began to become more stable.

Turbulent kinetic energy (TKE) is the kinetic energy of pulsation in the flow field, which reflects the intensity of turbulence and the energy loss of turbulent flow. That is, the energy in the mean-field is transferring out into turbulence production. The stability of the airflow can be derived from the magnitude of the TKE. The greater the TKE, the more energy is lost, so the pressure there is lower; that is, the pressure acting on the body surface by the rear of the car decreases, which eventually leads to the increase of pressure drag. Figure 11 plots the TKE distribution between the two bodies on the xz symmetry plane. It can be seen from this figure that the distribution shape of TKE between two bodies is very similar to the structural shape of wake between two bodies (Figure 7), and the peak of TKE is mostly distributed in the lower vortex region of the body wake. At $x/L = 0.25$, 0.5, and 0.75, the distribution of TKE (the value range is about 20–40) all covers the upper rounded edge of the trailing body's fore-body. With the increase of inter-vehicle distances, the flow interaction between the two bodies decreases, so its distribution on the fore-body of the trailing body becomes less.

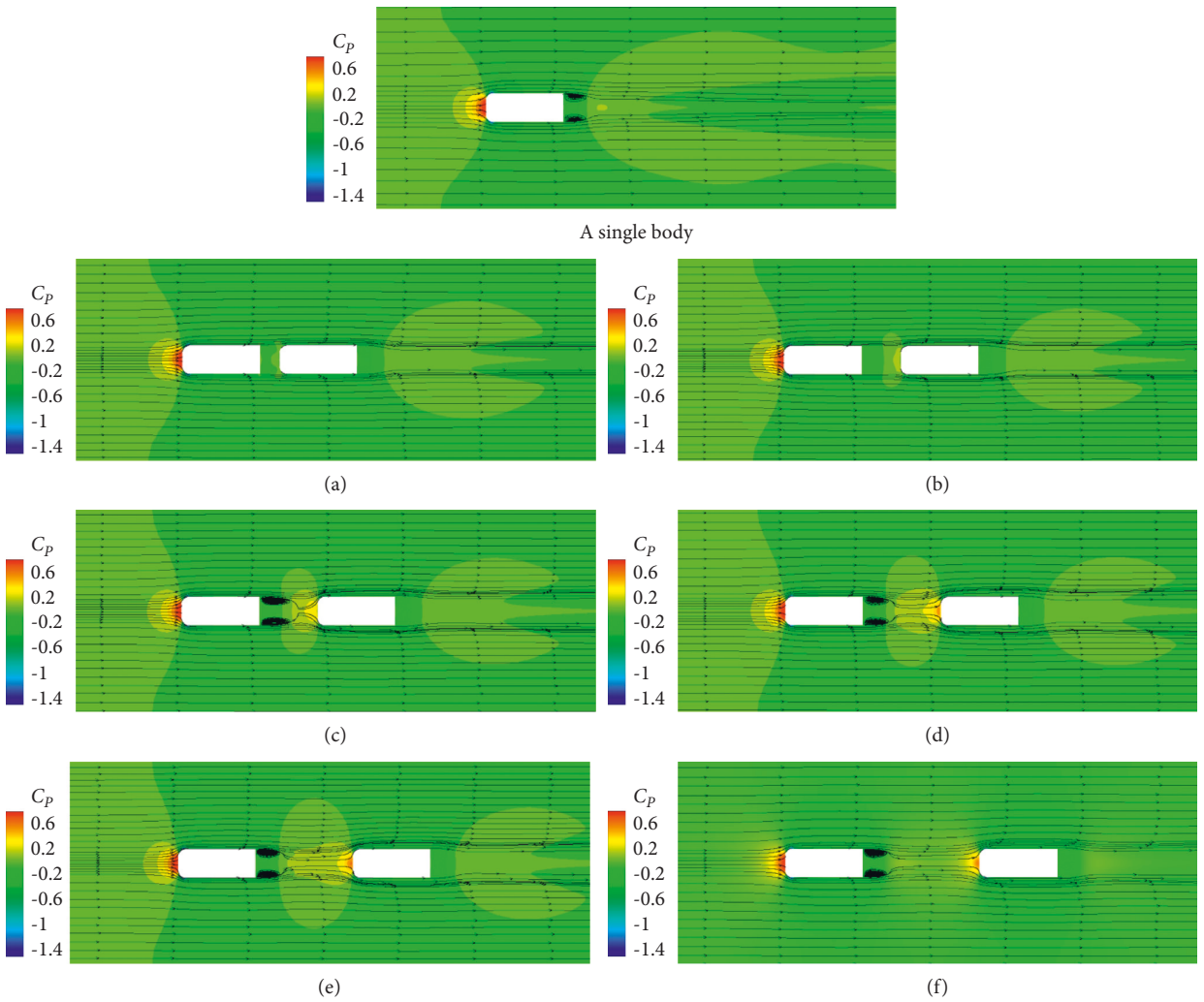

FIGURE 9: The pressure contour and streamline distribution of a single body and two bodies in the platoon on the z/(L) = 0.08 plane. (a) $x/L = 0.25$ (b) $x/L = 0.5$. (c) $x/L = 0.75$. (d) $x/L = 1$. (e) $x/L = 1.25$. (f) $x/L = 1.5$.

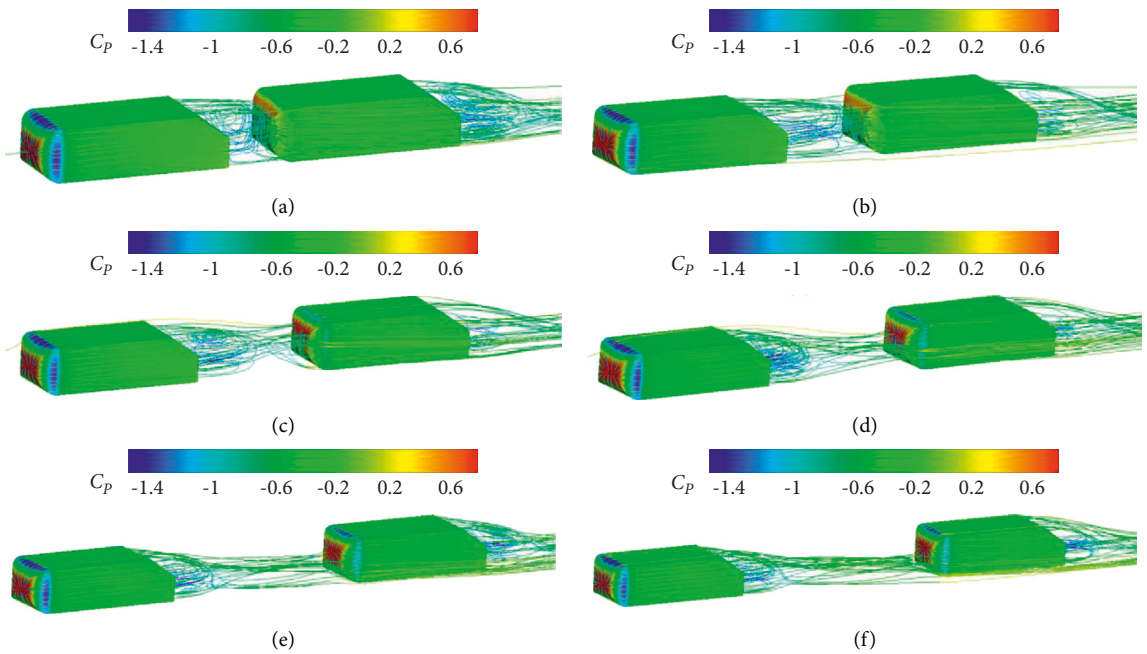

FIGURE 10: The static pressure and three-dimensional streamlines on the surfaces of two bodies under different inter-vehicle distances, where the three-dimensional streamlines are colored by the x-direction velocity. (a) $x/L = 0.25$ (b) $x/L = 0.5$. (c) $x/L = 0.75$. (d) $x/L = 1$. (e) $x/L = 1.25$. (f) $x/L = 1.5$.

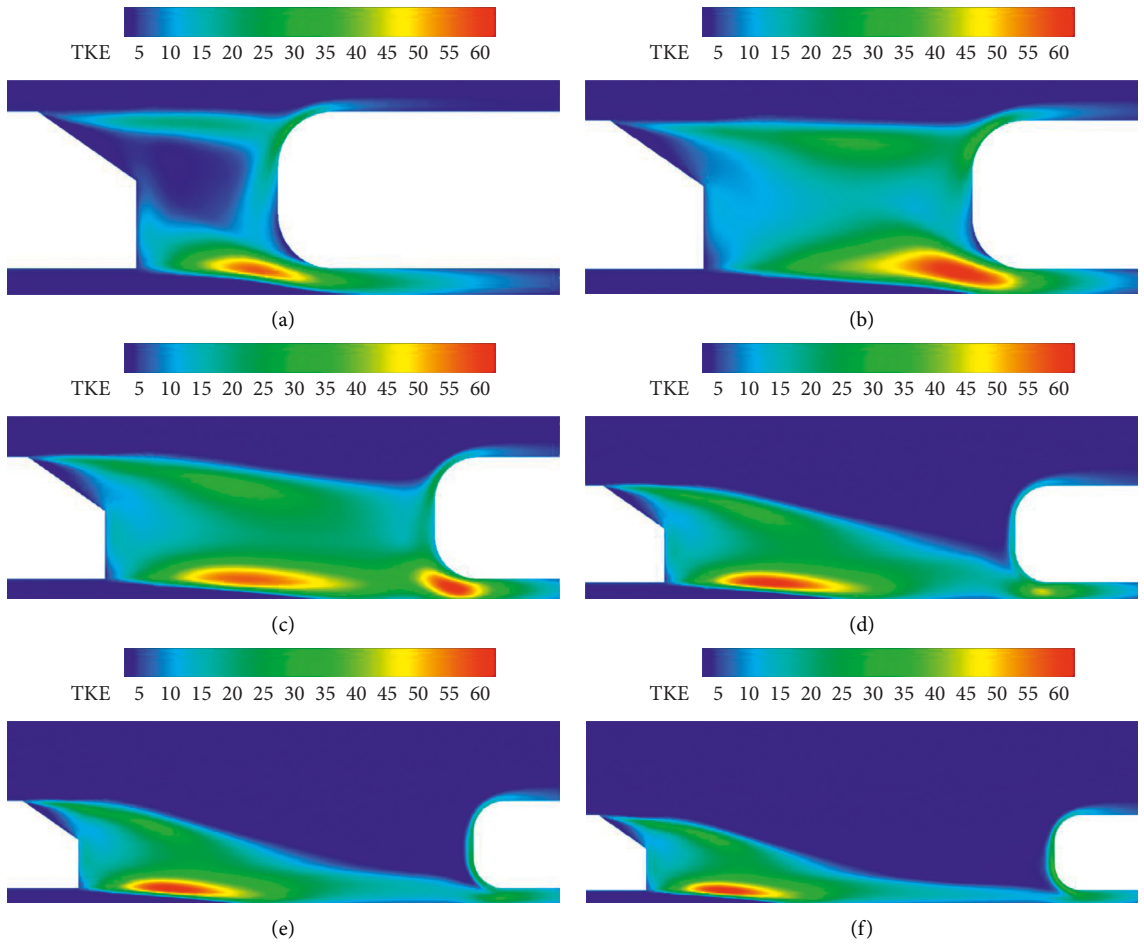

Figure 11: The distribution of TKE between two bodies at different inter-vehicle distances on the xz symmetry plane. (a) $x/L = 0.25$ (b) $x/L = 0.5$. (c) $x/L = 0.75$. (d) $x/L = 1$. (e) $x/L = 1.25$. (f) $x/L = 1.5$.

4.2. Three-Vehicle Platoon. The mesh generation, turbulence model, boundary conditions, and solution parameters of the three Ahmed bodies are consistent with the calculation method settings of single body. The inter-vehicle distance of the three-vehicle platoon simulation is $x/L = 0.25$–2.

Figure 12 shows the change of the drag coefficient of each body with $x/L = 0.25$ for 3, 4, 5, and 6 bodies in the platoon. It can be seen that increasing the number of vehicles in the platoon will not affect the change trend of vehicle drag coefficient in the platoon. For the last body in the platoon, with the increase of the number of bodies, the drag coefficient begins to decrease, because the flow field experienced by the following bodies has lower dynamic pressure and total pressure. With the increase of the number of bodies, the flow dissipation will be more and more, and the flow speed will be lower and lower. Taking into account the configuration of the computer this time, only the three-vehicle platoon is simulated here.

The effect of different inter-vehicle distances on the drag coefficient of the three bodies in the platoon is shown in Figure 13. At $x/L = 0.25$–1, the change trend of the drag coefficient of the leading body and the middle body in the platoon is very similar to that of the two bodies. This is the same as the result given in [34], which shows that increasing

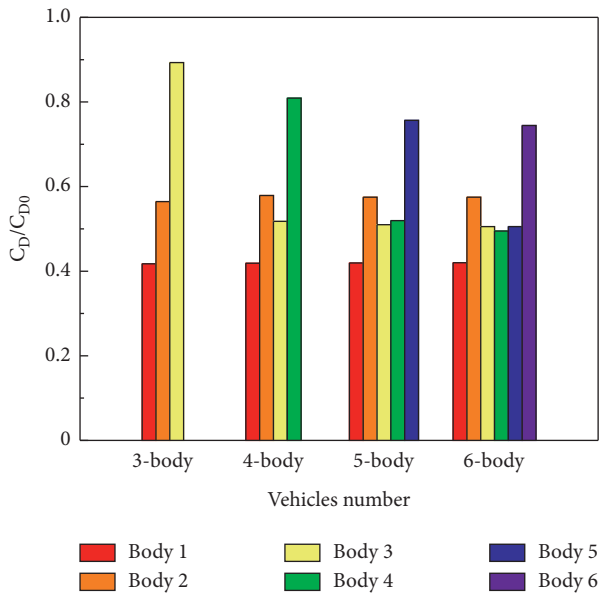

Figure 12: At x/(L) = 0.25, the comparison of the standardized drag coefficient C_D/C_{D0} of each body in the different numbers of vehicles in the platoon.

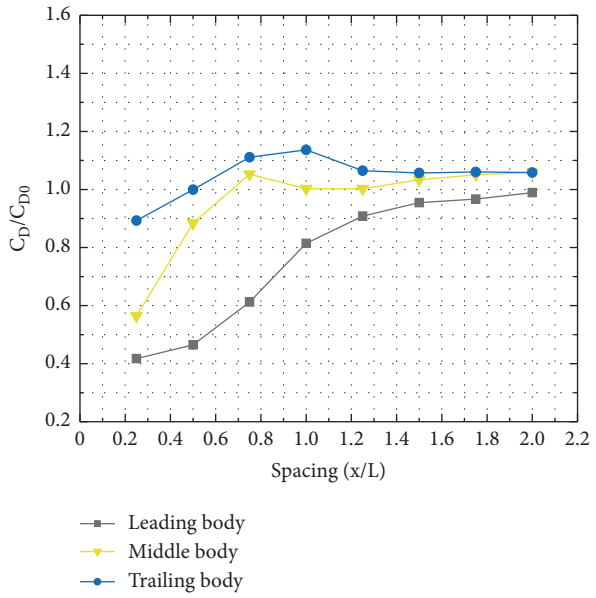

Figure 13: Normalized drag coefficient C_D/C_{D0} of three Ahmed bodies under different inter-vehicle distances.

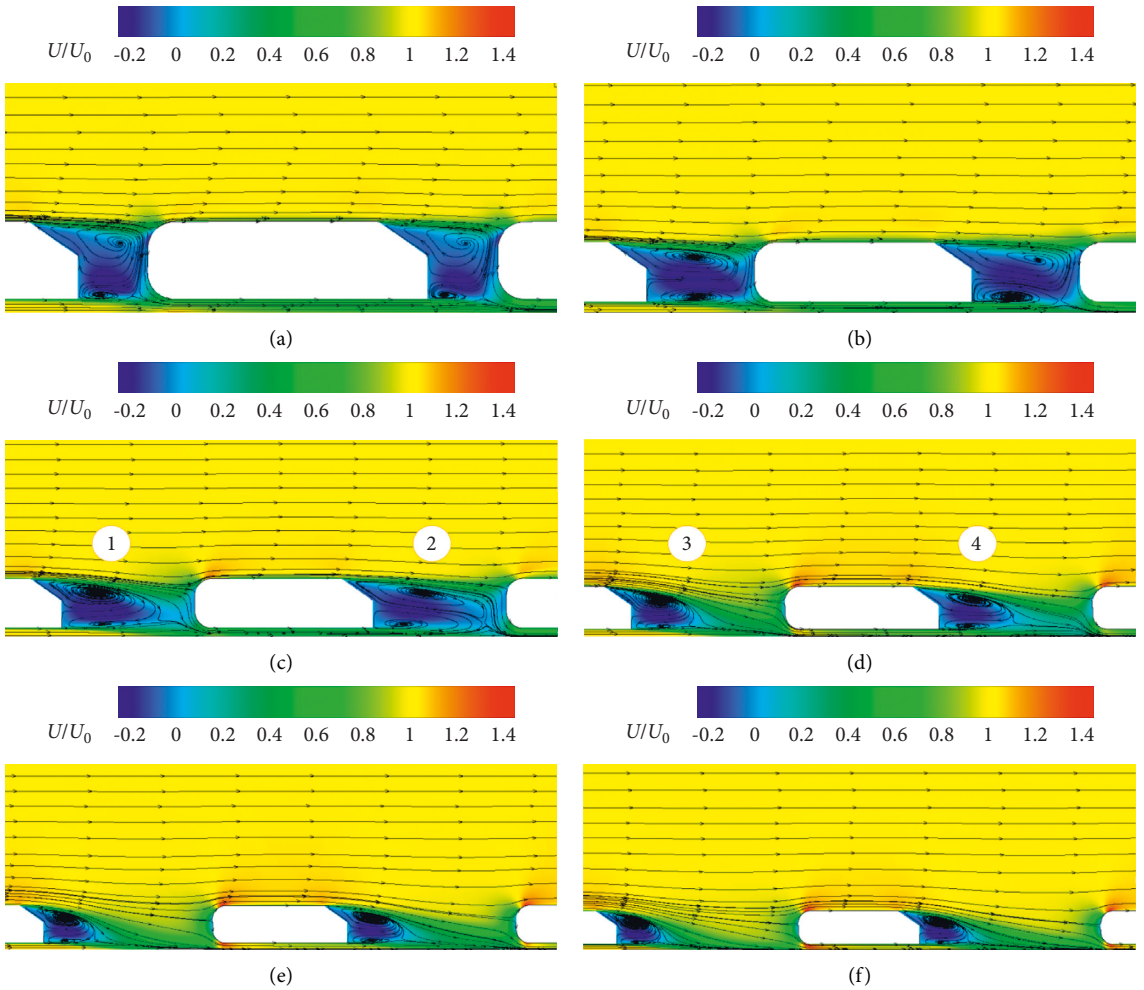

Figure 14: The x-direction velocity contour and streamline distribution between three bodies on the xz symmetry plane. (a) $x/L = 0.25$ (b) $x/L = 0.5$. (c) $x/L = 0.75$. (d) $x/L = 1$. (e) $x/L = 1.25$. (f) $x/L = 1.5$.

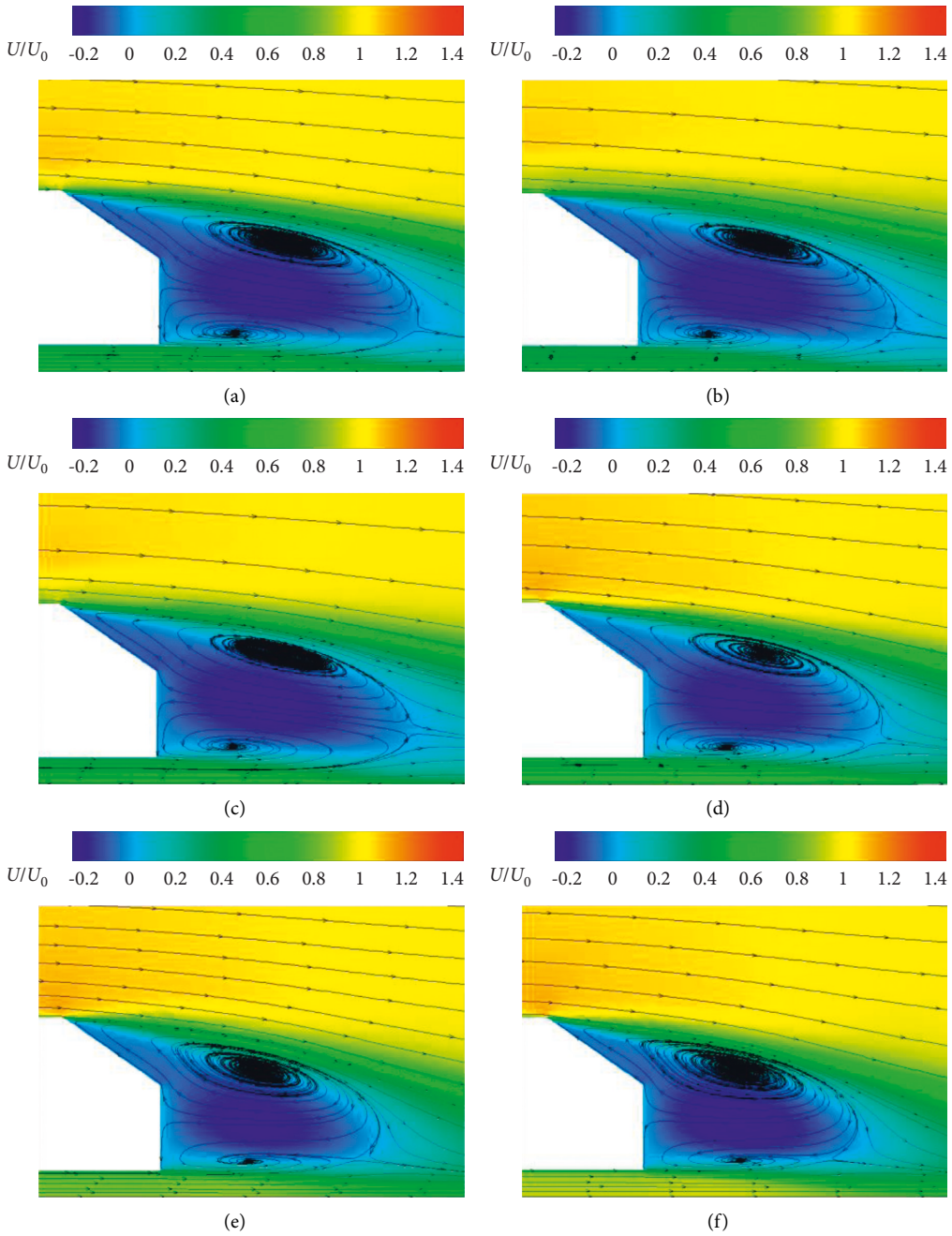

FIGURE 15: x-direction velocity contour and streamline distribution behind trailing body in three bodies on xz symmetry plane. (a) $x/L = 0.25$ (b) $x/L = 0.5$. (c) $x/L = 0.75$. (d) $x/L = 1$. (e) $x/L = 1.25$. (f) $x/L = 1.5$.

the number of bodies in the platoon will not affect the wake between the leading body and the middle body.

According to observations, for the leading body, whether it is in the case of three bodies or two bodies, the error of the drag coefficient between them is very small, almost the same. This is very consistent with the results observed in the literature [40]. In the range of the distance studied, the leading body always benefits from the platoon, and the drag coefficient is always lower than the value of a single body. When the spacing increases, the drag coefficient of the leading body starts to increase and approaches a single body value slowly until it is no longer affected by the following bodies.

It can also be seen from Figure 13 that for the middle body, the effects of both leading and trailing bodies are combined. When $x/L = 0.25$, the drag coefficient is very low, and this value is about 56% of the value of a single body. Then, when $x/L = 0.5$, the drag coefficient suddenly increases, and at this time it is still lower than the value of a single body. At the distance $x/L = 0.75$, the drag coefficient of the middle body reaches the highest value and is higher than

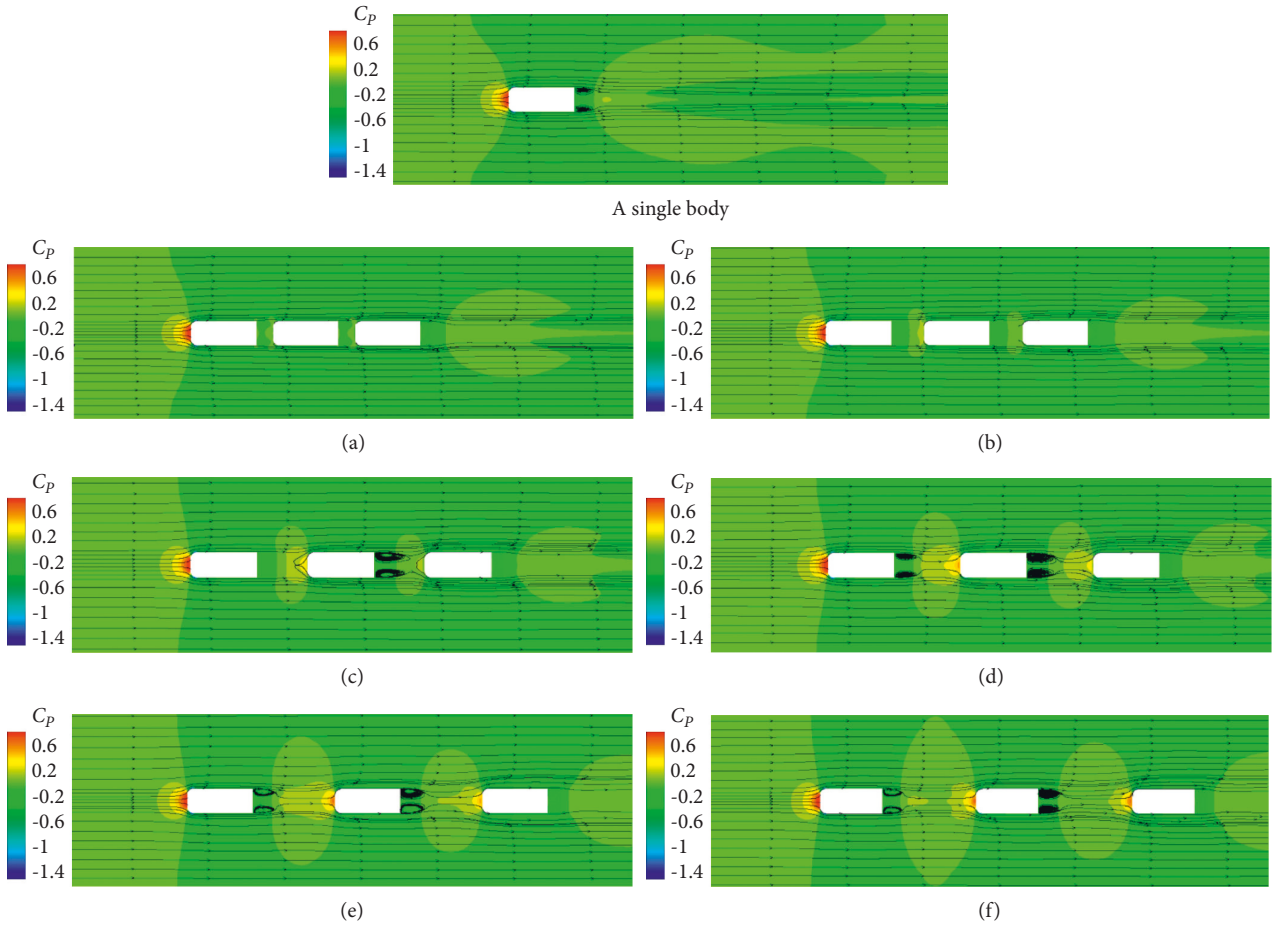

FIGURE 16: The pressure contour and streamline distribution of a single body and three bodies in the platoon on the z/(L) = 0.08 plane. (a) $x/L = 0.25$ (b) $x/L = 0.5$. (c) $x/L = 0.75$. (d) $x/L = 1$. (e) $x/L = 1.25$. (f) $x/L = 1.5$.

that of a single body. This should be related to the size of the wake between vehicles, which will be explained in the following wake structure analysis. Finally, as the spacing increases, the drag coefficient begins to slowly increase again; until $x/L = 2$, the drag coefficient of the trailing body and the middle body almost coincides. And after that, the drag coefficient of the trailing body will no longer be higher than that of the middle body (this can be seen from the following analysis of the change trend of the trailing body). Due to the limitation of the computer configuration, there is no simulation of the next inter-vehicle distances here.

For the trailing body, the drag coefficient keeps increasing in the range of $x/L = 0.5$–1 and is higher than the value of a single body. When the spacing increases to $x/L = 2$, the drag coefficient begins to decrease and approaches to the value of a single body.

In order to be consistent with the layout of the two-vehicle platoon analysis, the flow field, pressure field, and turbulent kinetic energy distribution are also given at six different inter-vehicle distances of $x/L = 0.25$, 0.5, 0.75, 1, 1.25, and 1.5.

At six different inter-vehicle distances, the x-direction velocity contours and streamline distributions of the xz symmetry plane between the three bodies (Figure 14) and behind the trailing body (Figure 15) are shown. It can be clearly seen from the figure that the overall change of the wake structure between bodies is very similar to the situation of two bodies. Especially when the distance $x/L = 0.25$–0.75, the drag coefficient of the middle body increases sharply and reaches the peak value. At $x/L = 0.75$, it can be seen from Figure 15 that the vortex structure and size in wake 1 (leading body and middle body) and wake 2 (middle body and trailing body) are different, and the region of wake 2 is larger than that of wake 1, so the drag coefficient of the middle body varies greatly. For $x/L = 1$, there is no difference in vortex structure between wake 3 (leading body and middle body) and wake 4 (middle body and trailing body), but it can also be seen that the region of wake 4 is slightly larger than that of wake 3. Therefore, the drag coefficient of the trailing body does not decrease but increases at this spacing. With the increase of spacing, the next change is the same as the situation of the two bodies. For the three bodies in the platoon, in each spacing, the upper and lower vortex cores between the trailing body and the middle body are always smaller than those between the middle body and the leading body, and this should be caused by flow dissipation and momentum loss. The variation trend of Figure 15 is the same as that of Figure 8 and will not be repeated here. Figure 16 shows the pressure contour and streamline distribution of a single body and

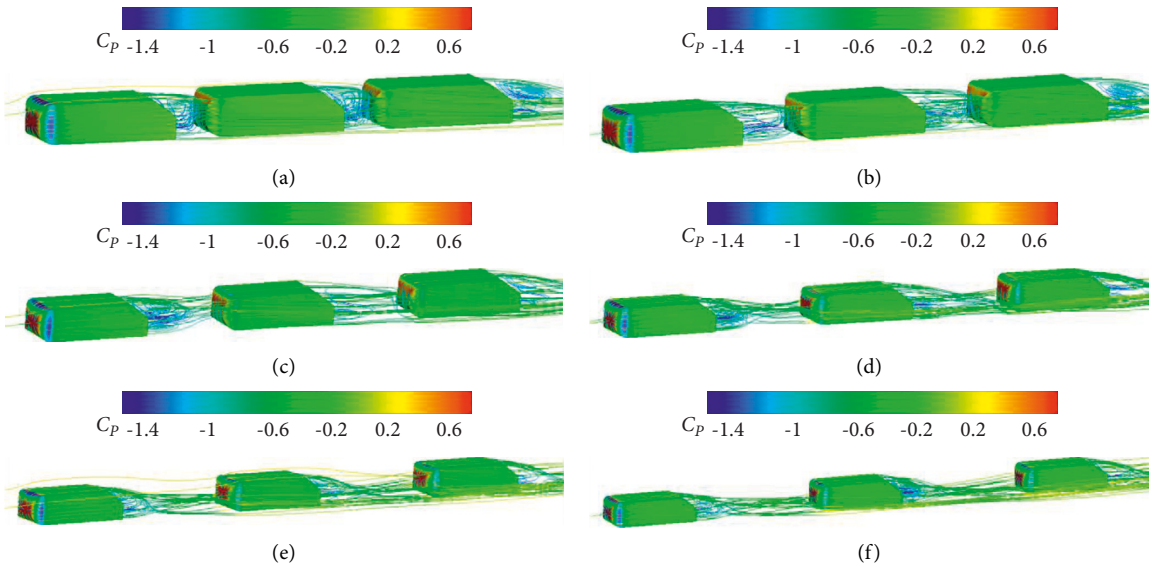

Figure 17: The static pressure and three-dimensional streamlines on the surfaces of three bodies under different inter-vehicle distances, where the three-dimensional streamlines are colored by the x-direction velocity. (a) $x/L = 0.25$ (b) $x/L = 0.5$. (c) $x/L = 0.75$. (d) $x/L = 1$. (e) $x/L = 1.25$. (f) $x/L = 1.5$.

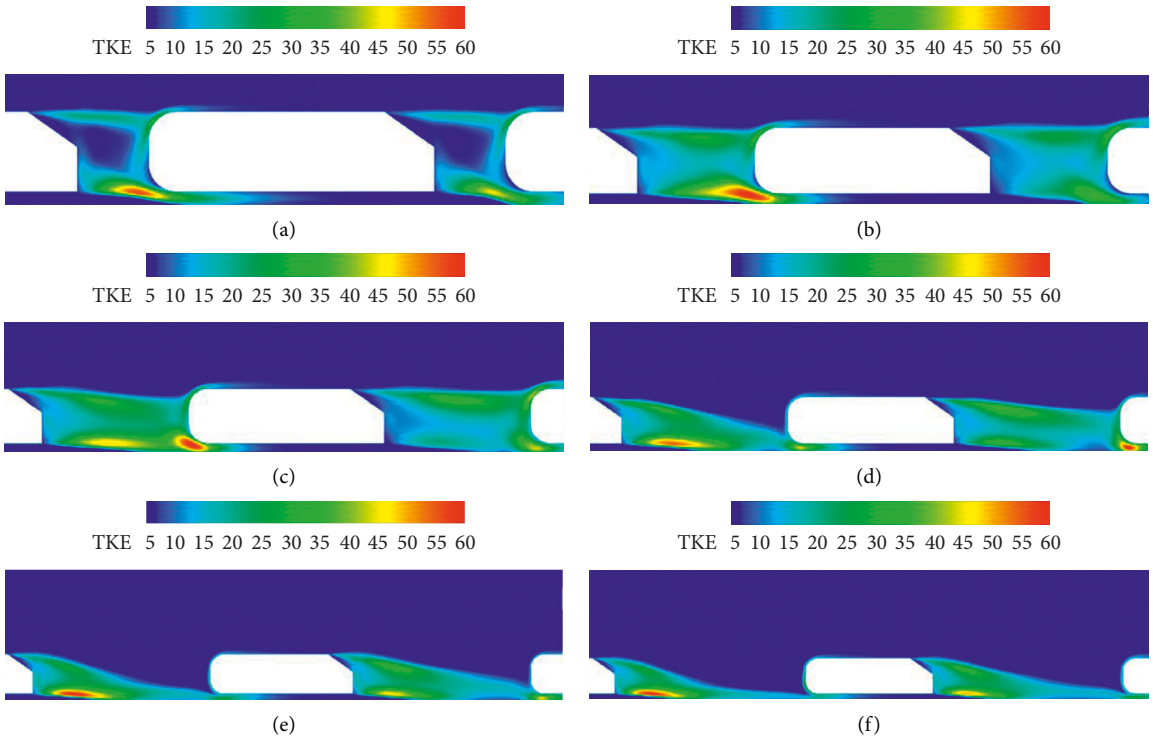

Figure 18: The distribution of TKE between three bodies at different inter-vehicle distances on the xz symmetry plane. (a) $x/L = 0.25$ (b) $x/L = 0.5$. (c) $x/L = 0.75$. (d) $x/L = 1$. (e) $x/L = 1.25$. (f) $x/L = 1.5$.

three bodies in the platoon on $z/L = 0.08$ plane, and the overall change is no different from the situation of two bodies. However, at $x/L = 0.75$, only the vortex appears in the wake of the middle body, which causes the drag coefficient of the middle body to increase sharply and is higher than a single body value.

The distribution of static pressure and turbulent kinetic energy acting on the surface of three bodies reported in Figure 17 and 18 is very similar to that observed in the platoon of two bodies. As shown in Figure 10, the three-dimensional wake structure observed in these areas hardly changes. In Figure 17, when the distance $x/L = 0.75$, the

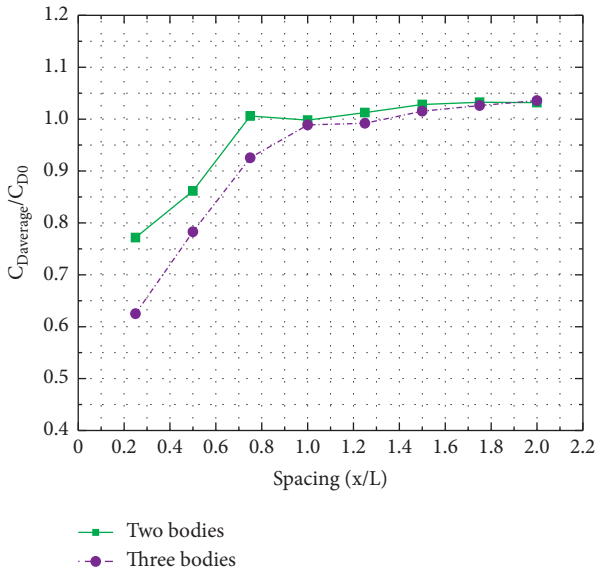

Figure 19: Comparison of the average drag coefficients of two bodies and three bodies.

flow impingement does not completely cover the center of the front surface of the middle body and the trailing body, which is somewhat different from the situation of the two bodies. However, at all distances, the static pressure distribution at the front of the middle body shows different changes from that of the trailing body, which is mainly due to flow dissipation and momentum loss. In Figure 18, at $x/L = 1$, the TKE (the value range is about 20–40) distributed on the fore-body of the trailing body is obviously more than that on the fore-body of the middle body, which also leads to the drag coefficient of the trailing body to be still high at this distance. At $x/L = 1.25$ and 1.5, it can be seen that there is no turbulent kinetic energy distribution on the fore-body of the middle body and the trailing body, and the three bodies become more like a single body.

In order to better show the drag reduction effect of the platoon vehicle, the averaged drag coefficient of the platoon is used to express, and the average value is defined as follows.

$$\frac{C_{\text{Daverge}}}{C_{D0}} = \left(\frac{1}{n}\right)\sum\left(\frac{C_{Di}}{C_{D0}}\right), \tag{7}$$

where i represents the ith vehicle in the platoon.

Figure 19 shows the comparison of the average drag coefficients of two bodies and three bodies. It is obvious from the figure that as the inter-vehicle distance decreases, the average drag coefficients of the two and three bodies are decreasing. The average drag coefficients of three bodies are lower than that of two bodies, although the distance $x/L = 2$ is opposite, because in the intelligent transportation system, the distance of 2 times the length of the vehicle is too far, which will not be considered in practical application. Therefore, the drag reduction effect of the three bodies is better than that of the two bodies, which can save fuel consumption better.

5. Conclusions

In this paper, the effect of aerodynamic characteristics of two bodies and three bodies under different inter-vehicle distances is described in detail by the steady-state numerical simulation method. First, the numerical simulation method of a single body is verified according to the existing experimental data, and then the drag coefficient, wake topology, surface pressure, and turbulent kinetic energy distribution of two and three bodies in the platoon are discussed. The main findings of this study are as follows:

(1) Using the RANS model to simulate a single 35° Ahmed body has obtained good results, but when simulating two 35° Ahmed bodies in the platoon, it is found that there is still a big error compared with the experimental data. This is because the steady-state RANS model is difficult to predict the three-dimensionality and unsteadiness of turbulence. Most people believe that although the instantaneous Navier–Stokes equation can be used to describe turbulence, the nonlinearity of the Navier–Stokes equation makes it extremely difficult to accurately describe all the details related to three-dimensional time with an analytical method.

(2) The increase from two bodies to three bodies will not affect the wake of the leading body. However, the drag of the middle body and trailing body is reduced compared to the single body in the platoon. The drag coefficient of the middle car is reduced by approximately 56% of the single car value at $x/L = 0.25$. With the increase in the number of vehicles, airflow impingement applied to the following vehicle is reduced, and the total drag is decreased. At $x/L = 0.75$, the drag coefficient of the middle body among the three bodies suddenly increases and reaches the highest value, which should be related to the size and structure of its wake, resulting in the decrease of the base pressure of the middle body. The research of various flow characteristics shows that the fundamental reason of the increase in the drag coefficient with $x/L = 0.25$–1 is the significant change of the flow structure between vehicles.

(3) From the comparison of the average drag coefficients of two bodies and three bodies in the platoon, increasing the number of vehicles in the platoon can indeed achieve the effect of drag reduction, thus saving fuel consumption. When the distance $x/L = 0.25$, the maximum averaged drag coefficient decreases by about 19%. Therefore, the vehicle model studied in this paper provides a theoretical reference for the aerodynamic characteristics of the increase in the number of vehicles in the platoon of the intelligent transportation system.

Data Availability

The data used to support the results of this study are included in the manuscript.

Conflicts of Interest

The authors declare that they have no conflicts of interest to this work.

Acknowledgments

This work was funded by the National Nature Science Foundation of China, under the research Grant nos. 51565006 and 52165055. This research was also supported by the Guangxi University of Science and Technology Doctoral Fund, under the research Grant 13Z10. It was also supported by the Guangxi Postgraduate Education Innovation Project (no.GKYC202114) and the Undergraduate Innovation and Entrepreneurship Training Program Project (no. 202110594178).

References

[1] H. K. Suh and C. S. Lee, "A review on atomization and exhaust emissions of a biodiesel-fueled compression ignition engine," *Renewable and Sustainable Energy Reviews*, vol. 58, pp. 1601–1620, 2016.

[2] Z. Zhang, J. Ye, D. Tan, Z. Feng, J. Luo, and Y. Tan, "The effects of fe2o3 based doc and scr catalyst on the combustion and emission characteristics of a diesel engine fueled with biodiesel," *Fuel*, vol. 290, no. 2, Article ID 120039, 2021.

[3] Z. Zhang, J. Ye, J. Lv et al., "Investigation on the effects of non-uniform porosity catalyst on SCR characteristic based on the field synergy analysis," *Journal of Environmental Chemical Engineering*, vol. 10, no. 1, Article ID 107056, 2022.

[4] T. Cai, S. M. Becker, F. Cao et al., "No emission performance assessment on a perforated plate-implemented premixed ammonia-oxygen micro-combustion system," *Chemical Engineering Journal*, vol. 417, Article ID 128033, 2021.

[5] T. Cai and D. Zhao, "Effects of fuel composition and wall thermal conductivity on thermal and nox emission performances of an ammonia/hydrogen-oxygen micro-power system," *Fuel Processing Technology*, vol. 209, Article ID 106527, 2020.

[6] Z. Zhang, J. Li, J. Tian et al., "The effects of Mn-based catalysts on the selective catalytic reduction of NOx with NH3 at low temperature: a review," *Fuel Processing Technology*, vol. 230, Article ID 107213, 2022.

[7] D. Zhao, Y. Guan, and A. Reinecke, "Characterizing hydrogen-fuelled pulsating combustion on thermodynamic properties of a combustor," *Communications on Physics*, vol. 2, no. 1, p. 44, 2019.

[8] D. Zhao, "Numerical investigation of a y-shaped thermoacoustic combustor with a helmholtz resonator implemented and operated at off-design conditions," *Journal of the Acoustical Society of America*, vol. 149, p. A141, 2021.

[9] T. Cai, D. Zhao, X. Li, B. Shi, and J. Li, "Mitigating NO emissions from an ammonia-fueled micro-power system with a perforated plate implemented," *Journal of Hazardous Materials*, vol. 401, Article ID 123848, 2021.

[10] M. Zabat, S. Frascaroli, and F. K. Browand, "Drag measurements on 2,3 and 4 car platoons," *SAE Technical Paper 940421*, p. 14, 1994.

[11] B. Blocken, Y. Toparlar, and T. Andrianne, "Aerodynamic benefit for a cyclist by a following motorcycle," *Journal of Wind Engineering and Industrial Aerodynamics*, vol. 155, pp. 1–10, 2016.

[12] H. Weimerskirch, J. Martin, Y. Clerquin, P. Alexandre, and S. Jiraskova, "Energy saving in flight formation," *Nature*, vol. 413, no. 6857, pp. 697-698, 2001.

[13] J. Katz, "Aerodynamics of race cars," *Annual Review of Fluid Mechanics*, vol. 38, no. 1, pp. 27–63, 2006.

[14] L. Tsuei and Ö. Savas, "A wind tunnel investigation of the transient aerodynamic effects on a four-car platoon during passing maneuvers," *SAE Technical Paper Series*, vol. 15, pp. 1470–1482, 2000.

[15] J. K. Hedrick, M. Tomizuka, and P. Varaiya, "Control issues in automated highway systems," *IEEE Control Systems Magazine*, vol. 14, no. 6, pp. 21–32, 1994.

[16] A. A. Alam, A. Gattami, and K. H. Johansson, "An experimental study on the fuel reduction potential of heavy duty vehicle platooning," in *Proceedings of the 13th International IEEE Conference on Intelligent Transportation Systems*, pp. 306–311, Funchal, Portugal, September 2010.

[17] C. Bonnet and H. Fritz, "Fuel consumption reduction experienced by two promote-chauffeur trucks in electronic towbar operation," in *Proceedings of the 7th World Congress On Intelligent Systems*, Turin, Italy, September 2000.

[18] S. Tsugawa, S. Kato, and K. Aoki, "An automated truck platoon for energy saving," in *Proceedings of the 2011 IEEE/RSJ International Conference on Intelligent Robots and Systems*, San Francisco, CA, USA, September 2011.

[19] R. Veldhuizen, G. Van Raemdonck, and J. van der Krieke, "Fuel economy improvement by means of two european tractor semi-trailer combinations in a platooning formation," *Journal of Wind Engineering and Industrial Aerodynamics*, vol. 188, pp. 217–234, 2019.

[20] M. He, S. Huo, H. Hemida et al., "Detached eddy simulation of a closely running lorry platoon," *Journal of Wind Engineering and Industrial Aerodynamics*, vol. 193, Article ID 103956, 2019.

[21] H. Humphreys and D. Bevly, "Computational fluid dynamic analysis of a generic 2 truck platoon," *SAE Technical Paper 2016-01-8008*, vol. 8, 2016.

[22] F. H. Robertson, F. Bourriez, M. He et al., "An experimental investigation of the aerodynamic flows created by lorries travelling in a long platoon," *Journal of Wind Engineering and Industrial Aerodynamics*, vol. 193, Article ID 103966, 2019.

[23] F. H. Robertson, D. Soper, and C. Baker, "Unsteady aerodynamic forces on long lorry platoons," *Journal of Wind Engineering and Industrial Aerodynamics*, vol. 209, Article ID 104481, 2020.

[24] P. Vegendla, T. Sofu, R. Saha, M. Madurai Kumar, and L. K. Hwang, "Investigation of aerodynamic influence on truck platooning," *SAE Technical Paper 2015-01-2895*, 2015.

[25] P. Schito and F. braghin, "Numerical and experimental investigation on vehicles in platoon," *SAE International Journal of Commercial Vehicles*, vol. 5, no. 1, pp. 63–71, 2012.

[26] D. Uystepruyst and S. Krajnović, "Les of the flow around several cuboids in a row," *International Journal of Heat and Fluid Flow*, vol. 44, pp. 414–424, 2013.

[27] W. Kim, J. Noh, and J. Lee, "Effects of vehicle type and inter-vehicle distance on aerodynamic characteristics during vehicle platooning," *Applied Sciences*, vol. 11, no. 9, 4096 pages, 2021.

[28] C. P. Bounds, S. Rajasekar, and M. Uddin, "Development of a numerical investigation framework for ground vehicle platooning," *Fluid*, vol. 6, no. 11, , p. 404, 2021.

[29] F. Jaffar, T. Farid, M. Sajid, Y. Ayaz, and M. J. Khan, "Prediction of drag force on vehicles in a platoon configuration

using machine learning," *IEEE Access*, vol. 8, pp. 201823–201834, 2020.

[30] S. P. Doppenberg, "Drag Influence of Tails in a Platoon of bluff Bodies," Master Thesis, Delft University of Technology, Delft, Netherlands, 2015.

[31] T. Gheyssens and G. Van Raemdonck, "Effect of the frontal edge radius in a platoon of bluff bodies," *SAE International Journal of Commercial Vehicles*, vol. 9, no. 2, pp. 371–380, 2016.

[32] G. Le Good, P. Boardman, M. Resnick, and B. Clough, "An Investigation of aerodynamic characteristics of three bluff bodies in close longitudinal Proximity," *SAE Technical Paper Series*, vol. 3, no. 6, pp. 2802–2830, 2019.

[33] G. Le Good, M. Resnick, P. Boardman, and B. Clough, "Effects on the aerodynamic characteristics of vehicles in longitudinal proximity due to changes in Style," *SAE Technical Paper Series*, 2018.

[34] H. Ebrahim and R. Dominy, "Wake and surface pressure analysis of vehicles in platoon," *Journal of Wind Engineering and Industrial Aerodynamics*, vol. 201, Article ID 104144, 2020.

[35] M. Zabat, *The Aerodynamic Performance of Platoon : Final Report*, California Path Research Report, CA, USA, 1995.

[36] M. Mirzaei, A. Pavlenko, S. Krajnovic, and V. G. Chernoray, "Experimental and numerical study of flow structures between two ahmed bodies with various inter-body distances," in *Proceedings of the Eighth International Symposium On Turbulence Heat and Mass Transfer*, pp. 835–838, Sarajevo, Bosnia, September 2015.

[37] R. M. Pagliarella, S. Watkins, and A. Tempia, "Aerodynamic performance of vehicles in platoons: the influence of backlight angles," *SAE Technical Paper Series*, vol. 1, no. 14, 2007.

[38] S. Watkins and G. Vino, "The effect of vehicle spacing on the aerodynamics of a representative car shape," *Journal of Wind Engineering and Industrial Aerodynamics*, vol. 96, no. 6-7, pp. 1232–1239, 2008.

[39] R. Pagliarella, *On the Aerodynamic Performance of Automotive Vehicle Platoons Featuring Pre and post-critical Leading forms*, Ph. D Thesis, RMIT University, Melbourne, Australia, 2009.

[40] C.-H. Bruneau, K. Khadra, and I. Mortazavi, "Flow analysis of square-back simplified vehicles in platoon," *International Journal of Heat and Fluid Flow*, vol. 66, pp. 43–59, 2017.

[41] M. Mirzaei and S. Krajnović, "Large eddy simulations of flow around two generic vehicles in a platoon," in *Proceedings of the 5th International Conference on Jets, Wakes and Separated Flows (icjwsf2015)*, pp. 283–288, Cham, July 2016.

[42] G. Rajamani, "Cfd analysis of air flow interactions in vehicle platoons," Masters Thesis, RMIT University, Melbourne, Australia, 2006.

[43] A. Altinisik, O. Yemenici, and H. Umur, "Aerodynamic analysis of a passenger car at yaw angle and two-vehicle platoon," *Journal of Fluids Engineering*, vol. 137, no. 12, 2015.

[44] F. Browand and M. Hammache, "The limits of drag behavior for two bluff bodies in tandem," *SAE Technical Paper 2004-01-1145*, 2004.

[45] D. Caridi, D. Cokljat, J. Schuetze, and R. Lechner, "Embedded large eddy simulation of flow around the ahmed body," *SAE International Journal of Commercial Vehicles*, vol. 5, no. 1, pp. 208–214, 2012.

[46] P. R. Spalart, W. H. Jou, M. Strelets, and S. R. Allmaras, *Comments on the feasibility of les for wings, and on a hybrid rans/les approach*, First AFOSR International Conference on DNS/LES, Ruston, LA, USA, 1997.

[47] A. Rao, G. Minelli, B. Basara, and S. Krajnović, "On the two flow states in the wake of a hatchback ahmed body," *Journal of Wind Engineering and Industrial Aerodynamics*, vol. 173, pp. 262–278, 2018.

[48] S. R. Ahmed, G. Ramm, and G. Faltin, "Some salient features of the time-averaged ground vehicle wake," *SAE Technical Paper Series*, vol. 34, Article ID 840300, 1984.

[49] H. Lienhart, C. Stoots, and S. Becker, "Flow and turbulence structures in the wake of a simplified car model (ahmed modell)," *New results in numerical and experimental fluid mechanics iii*, vol. 77, pp. 323–330, 2002.

[50] J. Eisma, J. Westerweel, G. Ooms, and G. E. Elsinga, "Interfaces and internal layers in a turbulent boundary layer," *Physics of Fluids*, vol. 27, no. 5, pp. 055103–055116, 2015.

[51] C. Y. Li, Z. Chen, T. K. T. Tse et al., "A parametric and feasibility study for data sampling of the dynamic mode decomposition: range, resolution, and universal convergence states," *Nonlinear Dynamics*, vol. 107, no. 4, pp. 3683–3707, 2022.

[52] T. Tunay, B. Sahin, and V. Ozbolat, "Effects of rear slant angles on the flow characteristics of ahmed body," *Experimental Thermal and Fluid Science*, vol. 57, pp. 165–176, 2014.

[53] P. Dančová, R. Gnatowska, and M. Sosnowski, "The influence of distance between vehicles in platoon on aerodynamic parameters," *EPJ Web of Conferences*, vol. 180, Article ID 02030, 2018.

[54] E. Serre, M. Minguez, R. Pasquetti et al., "On simulating the turbulent flow around the ahmed body: a French–German collaborative evaluation of les and des," *Computers & Fluids*, vol. 78, pp. 10–23, 2013.

[55] F. Delassaux, V. Herbert, I. Mortazavi, and C. Ribes, "Numerical investigation of the flow around a simplified ground vehicles using hybrid rans/les method," *Progress in Hybrid RANS-LES Modelling*, vol. 143, pp. 357–365, 2020.

[56] E. Guilmineau, G. B. Deng, A. Leroyer, P. Queutey, M. Visonneau, and J. Wackers, "Assessment of hybrid rans-les formulations for flow simulation around the ahmed body," *Computers & Fluids*, vol. 176, pp. 302–319, 2018.

[57] C. Hinterberger, M. García-Villalba, and W. Rodi, "Large eddy simulation of flow around the ahmed body," *The Aerodynamics of Heavy Vehicles: Trucks, Buses, and Trains*, vol. 19, pp. 77–87, 2004.

[58] S. Kapadia, S. Roy, M. Vallero, K. Wurtzler, and J. Forsythe, "Detached-eddy simulation over a reference ahmed car model," *Direct and Large-Eddy Simulation V*, vol. 9, pp. 481–488, 2004.

[59] P. J. Schmid, "Dynamic mode decomposition of numerical and experimental data," *Journal of Fluid Mechanics*, vol. 656, pp. 5–28, 2010.

[60] C. Y. Li, T. K. T. Tse, and G. Hu, "Dynamic mode decomposition on pressure flow field analysis: flow field reconstruction, accuracy, and practical significance," *Journal of Wind Engineering and Industrial Aerodynamics*, vol. 205, Article ID 104278, 2020.

[61] O. T. Schmidt, A. Towne, G. Rigas, T. Colonius, and G. A. Brès, "Spectral analysis of jet turbulence," *Journal of Fluid Mechanics*, vol. 855, pp. 953–982, 2018.

[62] A. Towne, O. T. Schmidt, and T. Colonius, "Spectral proper orthogonal decomposition and its relationship to dynamic mode decomposition and resolvent analysis," *Journal of Fluid Mechanics*, vol. 847, pp. 821–867, 2018.

[63] G. Berkooz, P. Holmes, and J. L. Lumley, "The proper orthogonal decomposition in the analysis of turbulent flows," *Annual Review of Fluid Mechanics*, vol. 25, no. 1, pp. 539–575, 1993.

[64] C. Y. Li, Z. Chen, T. K. T. Tse et al., "Establishing direct phenomenological connections between fluid and structure by the koopman-linearly time-invariant analysis," *Physics of Fluids*, vol. 33, no. 12, Article ID 121707, 2021.
[65] B. Herrmann, P. J. Baddoo, R. Semaan, S. L. Brunton, and B. J. McKeon, "Data-driven resolvent analysis," *Journal of Fluid Mechanics*, vol. 918, p. A10, 2021.
[66] A. F. Abdel Azim and A. F. Abdel Gawad, "A flow visualization study of the aerodynamic interference between passenger cars," *SAE Technical Paper 2000-01-0355*, 2000.